Supporting Information

Diaz-Horta et al. 10.1073/pnas.1401950111

SI Materials and Methods

Human Subjects. The study of hereditary hearing loss was approved by the Ethics Committee of Ankara University and the Institutional Review Board at the University of Miami. Informed consent was obtained from all participants or, in the case of minors, from the parents. Diagnosis of sensorineural hearing loss was established via standard audiometry in a soundproofed room according to current clinical standards. Hearing loss was classified according to GENDEAF guidelines (http://hereditaryhearingloss.org). Hearing impairment was additionally assessed by transient evoked otoacoustic emissions, immitancemetric measurements, and auditory brainstem response tests. Clinical evaluation of all affected individuals by a geneticist and an ear, nose, and throat surgeon included a thorough physical examination and otoscopy. The present study was performed in a large Turkish family with six members having profound sensorineural hearing loss (Fig. 1 *A* and *B*). Consanguinity was documented in one branch of the studied family; all other matings involved individuals from the same small town in Turkey, making it likely that they shared a common ancestor. DNA was extracted from blood via standard methods. One affected individual was prescreened and found to be negative for common causes of nonsyndromic deafness, including mutations in *GJB2* (MIM121011).

Whole-Exome Sequencing. Genomic DNA from one affected individual was used to sequence the whole exome. The SureSelect Human All Exon 50 Mb Kit (Agilent) was used for in-solution enrichment of coding exons and flanking intronic sequences following the manufacturer's standard protocol. Adapter sequences for the Illumina HiSeq 2000 were ligated and the enriched DNA samples were subjected to standard sample preparation for the HiSeq 2000 instrument. Paired-end reads of 99-base lengths were produced. The Illumina CASAVA v. 1.8 pipeline was used to produce 99-bp sequence reads. BWA (1) was used to align sequence reads to the human reference genome (hg19), and variants were called using the GATK software package (2, 3). All variants were submitted to SeattleSeq134 (http://snp.gs.washington.edu/SeattleSeqAnnotation134/) for further characterization.

The Genomes Management Application, University of Miami Miller School of Medicine (https://genomics.med.miami.edu/gem-app/), was used for filtering of variants. Whole-exome sequencing generated 73,634,276 reads. At 2-fold and 10-fold read depth, the coverage of targeted regions was 92.5% and 73.1%, respectively. The average read depth was 52.5-fold. The average quality of single-nucleotide variations (SNVs) and insertions or deletions (indels) was 687 and 1,001, respectively. Before applying any filter, 94,197 SNVs and 6,837 indels were found. The variants were filtered according to the inheritance model (autosomal recessive with both homozygous and compound heterozygous), the variant function class including missense, nonsense, splice sites, in-frame indels, and frame-shift indels, and the presence and frequency at the dbSNP137 (http://www.ncbi.nlm.nih.gov/projects/SNP/) and National Heart, Lung, and Blood Institute (http://evs.gs.washington.edu/EVS) databases (a minor allele frequency of less than 0.5% was used). For missense variants, we excluded those with both PolyPhen-2 (http://genetics.bwh.harvard.edu/pph2) and SIFT (http://sift.jcvi.org) prediction categories other than pathogenic as well as when the variant allele was present in more than one other sequenced species. We also filtered the variants that are present in more than five families in our internal database that includes 3,000 exomes from different ethnicities including 144 Turkish individuals. Mutations in all previously reported deafness genes were excluded as previously described (4).

Sanger Sequencing, RT-PCR, Genotyping, and Mutation Screening. The candidate variant observed via whole-exome sequencing was confirmed using conventional capillary sequencing (Fig. 1*C*). All primers (Table S1) were designed using Primer3, v. 0.4.0 (http://frodo.wi.mit.edu). PCR reactions included 20 ng of genomic DNA with Taq DNA polymerase (Roche). DNA fragments were amplified using primers FAM65B-F-908/FAM65B-R-908 and a touchdown protocol. PCR products were visualized on agarose gels and cleaned over Sephadex columns. Sequence analysis was performed with the ABI PRISM BigDye Terminator Cycle Sequencing v3.1 Ready Reaction Kit and the ABI PRISM 3730 DNA Analyzer (Applied Biosystems). Sequence traces were analyzed using Sequencher 4.7 software (Gene Codes).

To determine the effect of the splice site mutation on RNA splicing, total RNA was extracted from peripheral blood with a PAXgene Blood RNA Extraction Kit (Qiagen). cDNA synthesis from 1 μg of total RNA was performed using SuperScript III (Invitrogen) and random hexamers (Promega). For PCR, exonic primers (FAM65B-EXS-F/FAM65B-EXS-R) were designed to amplify a cDNA fragment from exons 2–6 (Table S1). Amplicons were then sequenced and traces were analyzed as described above.

To screen additional families for linkage to the *FAM65B* locus, rs4129512, rs9393592, rs4256430, and rs2747683 were genotyped with custom TaqMan probes (Applied Biosystems) in probands of 685 multiplex autosomal recessive and simplex families with nonsyndromic deafness after the identified splice variant was screened and found to be absent. For each TaqMan reaction, 20 ng DNA was mixed with TaqMan Universal PCR Master Mix (2×; Applied Biosystems) and SNP Genotyping Assay (20×; Applied Biosystems). PCR conditions were 50 °C for 2 min, 95 °C for 10 min, 40 cycles of 95 °C for 15 s, and 60 °C for 1 min. Data were analyzed with SDS 2.3 software (Applied Biosystems). All 22 coding exons and exon–intron boundaries of *FAM65B* (NM_014722.2, GenBank) were further screened via Sanger sequencing (using primers FAM65B-2-F/R to FAM65B-23F/R) in those individuals homozygous for the selected SNPs.

Animal Use. Wild-type male and female C57BL/6J mice, Sprague–Dawley rat pups, and Et(krt4:GFP)^{sqet4} zebrafish (5) were used in this study. All procedures were approved by the University of Miami Institutional Animal Care and Use Committee and followed the National Institutes of Health guidelines "Using Animals in Intramural Research (http://oacu.od.nih.gov/training/PI/main_menu.htm)."

***Fam65b* Expression in Mouse Tissue.** Quantitative PCR was used to assess mouse expression levels of *Fam65b* in heart, lung, brain, liver, kidney, and inner ear at embryonic day 15 ($n = 3$) and postnatal day 30 ($n = 3$). RNA was isolated from the abovementioned tissues using TRIzol (Life Technologies). One microgram of RNA was used to synthesize cDNA using SuperScript III and oligodT following the manufacturer's protocol (Life Technologies). Quantitative PCR was performed on an Applied Biosystems 7900HT using SYBR Green (Applied Biosystems) and a primer pair (mFam65b_all-f/r). All reactions were performed in duplicate following the amplification protocol 95 °C for 10 min, then 95 °C for 10 s, 58 °C for 30 s, and 72 °C for 30 s for 40 cycles. The relative expression level of *Fam65b* in each tissue was calculated with the ΔΔCt method (5) using *Gapdh* as

the housekeeping gene (primers: mGapdh-f/r; Table S1). For specificity assessment of *Fam65b* amplification, PCR products were subjected to Sanger sequencing.

Western Blotting. The longest product (isoform 1) of the mouse *Fam65B* gene is 1,087 amino acids long with an expected molecular weight of 119 kDa. Several isoforms resulting from alternative splicing have also been predicted (www.uniprot.org/uniprot/Q80U16). For Western blot analysis, six mouse cochleas were pooled and homogenized in 100 μL of protein extraction buffer (25 mM Tris·Cl, pH 7.4, 25 mM sodium citrate, 2% SDS, 5 mM $CaCl_2$, 0.5 mM DTT) plus 1:200 protease inhibitor mixture (Sigma). Ninety micrograms of each lysate was loaded onto precast 4–20% gradient SDS-polyacrylamide gels (Lonza) and transferred to a 0.2-μm PVDF membrane (Bio-Rad). Immunodetection was performed using a rabbit anti-FAM65B polyclonal antibody (1:800; Proteintech) or monoclonal mouse antibody (1:800; Novus Biologicals), with an acetyl-histone H3 antibody (1:5,000; Upstate) as loading control. The results were visualized by chemiluminescence using Pierce ECL Western Blotting Substrate (Thermo Scientific).

Whole-Mount Immunofluorescence of Rat Inner Ear. For whole-mount immunofluorescence of organ of Corti, 4-wk-old rat cochlea neuroepithelia were microdissected and fixed in 3% paraformaldehyde (PFA), permeabilized in 0.5% Triton X-100, and incubated overnight in blocking solution [5% (wt/vol) BSA in PBS]. Specimens were incubated with 1:500-diluted rabbit (Proteintech) or 1:400-diluted monoclonal mouse (Novus Biologicals) anti-FAM65B antibodies for 2 h at room temperature. After three PBS 1× washes, samples were incubated with anti-rabbit or anti-mouse Alexa Fluor 488 together with phalloidin-rhodamine (1:200; Molecular Probes, Life Technologies) for 1 h. After washing in PBS, inner ear neuroepithelia were mounted in ProLong Gold Antifade Reagent (Invitrogen) and imaged with a 63× objective with a Zeiss LSM 710 fluorescence microscope. Validation of the anti-FAM65B antibodies for specificity is shown in Fig. S1.

Generation of Wild-Type and Mutant *FAM65B* Expression Constructs. Wild-type *FAM65B* cDNA was synthesized from control blood RNA using SuperScript III (Invitrogen) and random hexamers (Promega). Full-length wild-type *FAM65B* lacking the stop codon was amplified by high-fidelity PCR using Long Expand Taq Polymerase (Roche) and a primer pair (TOPO-FAM65B-F/R; Table S1). The resulting amplicon was cloned into a pcDNA3.1/CT-GFP-TOPO vector (Invitrogen).

For the mutated variant lacking exon 3, cDNA from one affected individual was amplified by PCR (using primers FAM65B-TOPO-R and Seq1-FAM65B-2R) to generate a segment containing the two unique restriction ApaI and EcoRI sites located in *FAM65B* exons 2 and 8, respectively. The resulting segment was subcloned into a pCR2.1-TOPO vector (Invitrogen). The insert was removed with ApaI/EcoRI and cloned into the wild-type *FAM65B-GFP* construct. All constructs were verified by Sanger sequencing using primers Seq1-FAM65B-2R and Seq(1 to 7)-FAM65B-F.

Immunocytochemistry. To investigate the subcellular localization and expression pattern of wild-type and mutated FAM65B, 25% confluence African green monkey kidney fibroblast-like cell (COS7) monolayers cultured on coverslips and placed in six-well plates were transfected with the *FAM65B*-WT-*GFP* and *FAM65B*-MUT-*GFP* constructs using Lipofectamine 2000 (Invitrogen) following the manufacturer's standard instructions. Twenty-four hours posttransfection, cells were washed with PBS and fixed with 4% PFA/PBS solution. Cells were permeabilized with 0.5% Triton/PBS for 20 min, blocked with 5% BSA, and then immunopurified rabbit anti-FAM65 (Biosource) or mouse anti–β-tubulin (Sigma) was applied for 1 h. Specimens were washed with PBS, and anti-rabbit or anti-mouse Alexa Fluor 568 was applied, respectively. Specimens were either mounted in ProLong Gold Antifade Reagent with DAPI or further used for actin revelation using phalloidin-Alexa Fluor 647 and then mounted in ProLong Gold Antifade Reagent.

Madin–Darby canine kidney (MDCK II) cells were grown to 100% confluence and polarized on coverslips. They were double-transfected with constructs encoding FAM65B-GFP and untagged IL-2α receptor subunit using Lipofectamine 2000. After 24 h, cells were processed for immunocytochemistry using a similar procedure as for COS7 cells.

Biolistic Transfection of Rat Organotypic Hair Cells. Inner ear explants were transfected using a Helios gene gun as previously described (7) and incubated for 24 h for protein expression. Specimens were then fixed with 3% PFA, permeabilized with 0.5% Triton X-100, and counterstained with rhodamine-phalloidin and mounted with ProLong Gold Antifade Reagent. Preparations were imaged using a 63× objective with a Zeiss LSM 710 fluorescence microscope.

Molecular Modeling. A structural model of the PX–BAR module (residues 1–300) of human FAM65B was built using MODELER software based on homology modeling (8). Forty-four percent of residues within the putative PX–BAR module of FAM65B display strong sequence similarity, as determined by Clustal W (9), to the canonical PX–BR module of SNX33. Briefly, the crystal structure of the PX–BAR module of human SNX33 (Protein Data Bank ID code 4AKV, the sorting nexin 33, was used as a template. A total of 100 atomic models was calculated and the structure with the lowest energy, as judged by the MODELER Objective Function, was selected for further analysis. The structural model was rendered using RIBBONS (10), and the electrostatic surface potential map was generated using MOLMOL (11).

Zebrafish *fam65b* in Situ Hybridization and Morpholino Knockdown. The zebrafish ortholog of human *FAM65B* (OTTDARG00000017115) is located on chromosome 19. The reported transcript (OTTDART00000020627) contains 22 exons. Human and zebrafish FAM65B proteins are 56% identical. However, in the first 362-amino acid segment that contains the PX–BAR module, the identity increases up to 78%.

To determine the expression pattern of *fam65b*, in situ hybridization experiments were conducted on whole-mount zebrafish as previously described (12). Two sets of DIG-tagged antisense and sense probes were synthesized by PCR using the primers zISH_T3FAM1-f/zISH_T7FAM1-r and zISH_T3FAM2-f/zISH_T7FAM2-r, followed by in vitro transcription using a DIG-RNA labeling mix (Roche) and T3 or T7 RNA polymerases (Promega). At least seven zebrafish larvae were tested for each probe.

To generate zebrafish larvae with reduced fam65b function, we designed two splice-blocking morpholinos, MO1 and MO2 (Table S1) (GeneTools,) targeting the intron 2–exon 3 and exon 3–intron 4 junctions, respectively. The efficacy of *fam65b* knockdown by both morpholinos was assessed by RT-PCR of morpholino-induced exon 3 skip, intron 2 retention, or intron 3 retention using the primer pairs Fam65b_f_exon sz/Fam65b_r_exon sz, zFAM_I2R_F/zFAM_I2R_R, and zFAM_I3R_F/zFAM_I3R_R, respectively. Briefly, total RNA was extracted from 3 days post-fertilization (dpf) embryos using TRIzol (Life Technologies) and treated with DNase I (Invitrogen). One microgram of purified RNA was reverse-transcribed to cDNA using oligodT and SuperScript III (Life Technologies). One microliter cDNA was then used as a template for PCR reactions. β-Actin was used as

the reference gene and was amplified using the primers Z_BActin-f and Z_BActin-r. MO1 and MO2 were titrated to determine the lowest dose (0.125 mM in 5 nL for both morpholinos) that induced missplicing events. For phenotypic assessment, MO1 and MO2 morphants were compared with stage-matched control zebrafish injected with the same concentration of a control morpholino (COMO) (Table S1) (GeneTools).

For quantification of neuromasts and saccular hair cells, Et(krt4:GFP)^{sqet4} zebrafish with GFP expression in hair cells were examined at 3 dpf. Zebrafish were fixed in 4% PFA at 4 °C for 2 h and then rinsed three times for 10 min each in PBS. To visualize hair cells in the saccular epithelium, the saccular otolith was dissolved in 0.5% Triton X-100 for 2 h at room temperature (13). Zebrafish larvae were positioned laterally in Vectashield antifading solution in 35-mm MatTek dishes. Images of hair cell bodies in both the otic vesicles and neuromasts were taken at 40× using confocal microscopy. After 3D reconstruction of hair cells was made with Nikon EC1 software, the number of hair cells in each saccular epithelium and the number of neuromasts on each lateral side were counted.

Microphonic potential recording was used to assess hearing of larval zebrafish (14). Briefly, 3-dpf zebrafish were anesthetized in 0.01% buffered MS-222 solution (Sigma) and embedded dorsal up in the same solution containing 1.8% agarose in 35-mm MatTek dishes. A MatTek dish with a larva was then placed in a temperature-controlled stage (28.5 °C) under a Zeiss Axioskop 2 FS Plus microscope. The microscope setup rested on an antivibration table electrically shielded by a Faraday cage. This entire setup was enclosed in an acoustic booth.

A glass stimulus probe with a tip size of 20 mm in diameter was driven by a piezoelectric actuator and the displacement of the probe at 200 Hz was calibrated. The probe tip was placed against the posterior edge of the otic vesicle of the fish and provided linear oscillatory motion along an axis parallel to the longitudinal axis of the fish body. A beveled micropipette with resistance between 4 and 6 MΩ was inserted into the otic vesicle to record the microphonic potential response from hair cells. Microphonic responses were amplified 1,000×, band pass-filtered between 0.1 and 3,000 Hz, and averaged 200 times. The amplitude of microphonic waveforms in response to 200-Hz stimulation at 5.8-μm displacement was measured in root mean square. Microphonic responses were recorded as stimulus displacement gradually decreased at a step of 3 dB until the threshold was reached. Threshold was defined as the lowest stimulus displacement that generated a microphonic response in the fast Fourier transform plot with a peak at 400 Hz that was just higher than the background noise level.

1. Li H, Durbin R (2010) Fast and accurate long-read alignment with Burrows-Wheeler transform. *Bioinformatics* 26(5):589–595.
2. McKenna A, et al. (2010) The Genome Analysis Toolkit: A MapReduce framework for analyzing next-generation DNA sequencing data. *Genome Res* 20(9): 1297–1303.
3. DePristo MA, et al. (2011) A framework for variation discovery and genotyping using next-generation DNA sequencing data. *Nat Genet* 43(5):491–498.
4. Diaz-Horta O, et al. (2012) Whole-exome sequencing efficiently detects rare mutations in autosomal recessive nonsyndromic hearing loss. *PLoS ONE* 7(11):e50628.
5. Parinov S, Kondrichin I, Korzh V, Emelyanov A (2004) Tol2 transposon-mediated enhancer trap to identify developmentally regulated zebrafish genes in vivo. *Dev Dyn* 231(2):449–459.
6. Livak KJ, Schmittgen TD (2001) Analysis of relative gene expression data using real-time quantitative PCR and the 2(-Delta Delta C(T)) Method. *Methods* 25(4): 402–408.
7. Grati M, et al. (2012) Localization of PDZD7 to the stereocilia ankle-link associates this scaffolding protein with the Usher syndrome protein network. *J Neurosci* 32(41): 14288–14293.
8. Martí-Renom MA, et al. (2000) Comparative protein structure modeling of genes and genomes. *Annu Rev Biophys Biomol Struct* 29:291–325.
9. Larkin MA, et al. (2007) Clustal W and Clustal X version 2.0. *Bioinformatics* 23(21): 2947–2948.
10. Carson M (1991) RIBBONS 2.0. *J Appl Crystallogr* 24(Pt 5):958–961.
11. Koradi R, Billeter M, Wüthrich K (1996) MOLMOL: A program for display and analysis of macromolecular structures. *J Mol Graph* 14(1):51–55, 29–32.
12. Thisse C, Thisse B (2008) High-resolution in situ hybridization to whole-mount zebrafish embryos. *Nat Protoc* 3(1):59–69.
13. Lu Z, DeSmidt AA (2013) Early development of hearing in zebrafish. *J Assoc Res Otolaryngol* 14(4):509–521.
14. Yariz KO, et al. (2012) Mutations in OTOGL, encoding the inner ear protein otogelin-like, cause moderate sensorineural hearing loss. *Am J Hum Genet* 91(5):872–882.

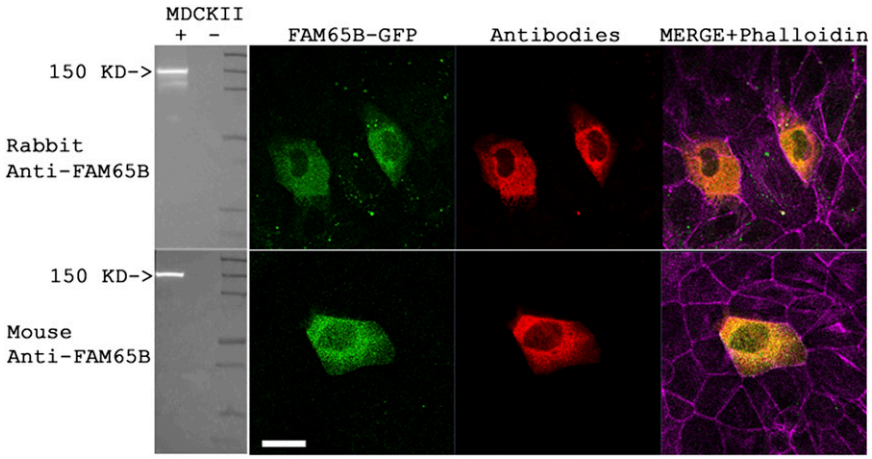

Fig. S1. Validation of FAM65B antibodies. We used a rabbit polyclonal anti-FAM65B antibody (Proteintech) and a monoclonal antibody (Novus Biologicals), the specificity of which was validated by Western blotting of protein extracts from MDCK II cells expressing wild-type FAM65B-GFP (*Left*) and by immunocytochemistry (*Right*). The immunogens used consist of 387 amino acids of the FAM65B C terminus and the first 592 amino acids of the FAM65B N terminus, respectively. (Scale bar, 5 μm.)

Table S1. Primers and morpholinos for *FAM65B* analysis

Name	Sequence, 5′ to 3′	Amplicon size, bp
FAM65B-F-908	ACCCCTTGGGTCTTTCCTTA	366
FAM65B-R-908	TTCAAGGCTGCAGTGAGCTA	
FAM65B-EXS-F	GCCCAATGGGATCATTAGAA	367
FAM65B-EXS-R	AAACTCCAGGCGTCTCATGT	
FAM65B_2-F	CATCTTCTGTCTGAACCTGCC	238
FAM65B_2-R	TCAAAGTTCACTTCCTTGGC	
FAM65B_3-F	TTGGTCAAATCCTTTTGGATG	260
FAM65B_3-R	ACCCCTTGGGTCTTTCCTTA	
FAM65B_4-F	ACAGGCGCAGAGATTACGAT	195
FAM65B_4-R	GCCCCATCCAGTAAAAGAAG	
FAM65B_5-F	AAACATCCAGTAGAATTTTGTAGGG	282
FAM65B_5-R	CTCAAGTGATCCACCCACCT	
FAM65B_6-F	ATCAAGATATTCTCACAAGCCTAAG	194
FAM65B_6-R	CCAAAGGTGTATTTGATTAGCAAC	
FAM65B_7-F	TGATCTATGTATTTTCTTTCAAGCC	273
FAM65B_7-R	ACCAACAATTCACACCAGGC	
FAM65B_8-F	AACGTCGTGTGCTTTGAGC	194
FAM65B_8-R	TCAAGGAGCTCTGCACTCTG	
FAM65B_9-F	TTTTAACGTGCCAGTATGTGTC	195
FAM65B_9-R	GCAAAATAATGACATGACAACTG	
FAM65B_10-F	TGTTCTGGTGGAGAAGAGGG	256
FAM65B_10-R	GTAAGGGCCCCACCAATG	
FAM65B_11-F	TGAAAGAAATGACCAACCTAGC	323
FAM65B_11-R	GCACCAGCTTTGAGTAGCAC	
FAM65B_12-F	GTGATTTTGCCAAATGTGC	243
FAM65B_12-R	TTCAAATGCTGGGTGCAAG	
FAM65B_13-F	AGCTAACAAAATGTAGTAACCTGATTC	277
FAM65B_13-R	AAGTCACACATGCCACAAGC	
FAM65B_14.1-F	CACACACGGCATCAACAAAT	544
FAM65B_14.1-R	TGCTTCTGCAACATCATTCTC	
FAM65B_14.2-F	GAGGAGCCCAGAAAACCTG	463
FAM65B_14.2-R	TGTTGGCTTAGGACACCTCTC	
FAM65B_15-F	CGTGTGTCTGGTTTCTCTTTC	322
FAM65B_15-R	CCCCTCTGACAGTAACAAAGAAC	
FAM65B_16-F	AAAGTAGAGAAAGAACTTTGAAAGCAA	493
FAM65B_16-R	CTCATTTCCCTGGCAACACT	
FAM65B_17-F	GGAAGAAAAACATCGCATGA	383
FAM65B_17-R	AGTGGACTGGGCTAGTGGTG	
FAM65B_18-F	GAGCTGAGATCATGCCATTG	334
FAM65B_18-R	TGCCCACTCTCACACTGAAG	
FAM65B_19-F	AACCTGGGCAACAAAGTGAG	372
FAM65B_19-R	AGGCCATCATTGCCAAAAG	
FAM65B_20-F	GCATAGTCTGTCCTTTTCTCACC	560
FAM65B_20-R	GGGGCTGGACTTAAGGGG	
FAM65B_21-F	GTATACCTCTTAAACTACGAACAAACC	204
FAM65B_21-R	CTCAGCTTAGCCTGGCTCC	
FAM65B_22-F	TTGTGAAATGCCAAGTCTCG	292
FAM65B_22-R	AGCGGGGAAACTGCTAAAC	
FAM65B_23-F	GCATATTATAGCAACCCATCCC	264
FAM65B_23-R	CACCATCCTGATGAAAAGGG	
FAM65B-TOPO-F	CAGACTCCCGGAAATCATGT	3221
FAM65B-TOPO-R	GAAAGGCTGTGGCAACTTCAG	
Seq1-FAM65B-2R	CCAGCCAGACCTTTCATCTT	645 with FAM65B-TOPO-F
Seq1-FAM65B-r	ACCCAGGCGAGAGTTTCTTT	—
Seq2-FAM65B-f	AGGGCCTTGAAAAATGGACT	—
Seq3-FAM65B-f	TTTCTGCCCCTGATAGTTGG	—
Seq4-FAM65B-f	CCTCACCTCCCACTCAACAG	—
Seq5-FAM65B-f	TGAAGGCTGCAGATCCTTTC	—
Seq6-FAM65B-f	TCCAAGTGATGGAGAAACTCG	—
Seq7-FAM65B-f	CAAACCATGAGTGACCTTGC	—

Table S1. Cont.

Name	Sequence, 5′ to 3′	Amplicon size, bp
mFam65b_all-f	GGGCTTGATGAGTACCTGGA	240
mFam65b_all-r	GAAGGCTTGCTTCATTTTGC	
mGapdh-f	CAACTTTGTCAAGCTCATTTCCTG	130
mGapdh-r	TCAGTGTCCTTGCTGGGGTG	
Fam65b_f_exon sz	TCATCAGGAGCCAGTCGTTC	400/235
Fam65b_r_exon sz	AAGCCCTCGTACAGCTCATC	
zFAM_I2R_F	GCAAAGTTTTCTTTAAGCATCC	246
zFAM_I2R_R	CACGTTTAGGCTGTGGCTCT	
zFAM_I3R_F	GTGCAGAAGAAGCCCATCTC	236
zFAM_I3R_R	TTGTAAAGTTAAAACATTTAAGGCAAT	
zISH_T3FAM1-f	CATTAACCCTCACTAAAGGGAAGAGGCCTCGACTTCAATATCA	367
zISH_T7FAM1-r	TAATACGACTCACTATAGGGAAGGCTCCGTCCAAAGAAAT	
zISH_T3FAM2-f	CATTAACCCTCACTAAAGGGAACACGTGCTGTCTTCTTTGACA	395
zISH_T7FAM2-r	TAATACGACTCACTATAGGGGCTGCAGTCGGACCATAGAG	
Z_BActin-f	CGAGCTGTCTTCCCATCCA	86
Z_BActin-r	TCACCAACGTAGCTGTCTTTCTG	
COMO	CCTCTTACCTCAGTTACAATTTATA	—
MO1	TGCACCTGAAGACACGCAGACAGAT	—
MO2	ATATCTAGCAGCACTTACTCCAGGC	—

The letters F or f and R or r in the primer names indicate forward and reverse, respectively.